Measurements of the Cross-Bridge Attachment/Detachment Process within Intact Sarcomeres by Surface Plasmon Resonance†

Carl W. Tong,‡ Alexander Kolomenskii,§ Vladimir A. Lioubimov,§ Hans A. Schuessler,§ Andreea Trache,‡ Harris J. Granger,‡ and Mariappan Muthuchamy*,‡

Cardiovascular Research Institute and Department of Medical Physiology, College of Medicine, Texas A&M University System Health Science Center, 336 Reynolds Medical Building, College Station, Texas 77843-1114, and Department of Physics, Texas A&M University, College Station, Texas 77843-4242

Received January 25, 2001; Revised Manuscript Received September 10, 2001

ABSTRACT: We have developed a surface plasmon resonance (SPR) system to monitor the cross-bridge attachment/detachment process within intact sarcomeres from mouse heart muscle. SPR occurs when laser light energy is transferred to surface plasmons that are resonantly excited in a metal (gold) film. This resonance manifests itself as a minimum in the reflection of the incident laser light and occurs at a characteristic angle. The angle of the SPR occurrence depends on the dielectric permittivity of the sample medium adjacent to the gold film. Purified sarcomeric preparations are immobilized onto the gold film in the presence of a relaxing solution. Replacement of the relaxing solution with increasing Ca^{2+} concentration solution activates the cross-bridge interaction and produces an increase in the SPR angle. These results imply that the interaction of myosin heads with actin within an intact sarcomere changes the dielectric permittivity of the sarcomeric structure. In addition, we further verify that SPR measurements can detect the changes in the population of the attached cross-bridges with altered concentrations of phosphate, 2,3-butanedione monoxime, or adenosine triphosphate at a fixed calcium concentration, which have been shown to reduce the force and increase the cross-bridge population in attached state. Thus, our data provide the first evidence that the SPR technique allows the monitoring of the cross-bridge attachment/detachment process within intact sarcomeres.

The attachment of myosin to actin initiates the conversion of stored chemical energy to mechanical force production in smooth, skeletal, and cardiac muscles. Regulation of the cross-bridge attachment/detachment process in cardiac muscle involves steric, allosteric, and cooperative mechanisms within sarcomeric proteins of the thick (myosin heavy chain, myosin light chain, and myosin binding protein C) and thin [actin, tropomyosin (TM), and troponin complex] filaments. Calcium binding to troponin C (TnC) triggers an allosteric effect on troponin I (TnI) and troponin T (TnT) to allow TM to flex (as reviewed in ref *1*). This causes TM to move away from its steric hindering position, allowing cross-bridge formation through the attachment of myosin heads to actins. The transition from a weakly bound cross-bridge to a strongly bound state locks TM in an open position; this produces a cooperative effect of promoting further cross-bridge attachment (*2*−*6*). After generation of a power stroke, the actomyosin interaction shifts to a rigor state. Subsequent adenosine triphosphate (ATP) binding then promotes the detachment process (*7*). β-Adrenergic stimulation increases the frequency of the cross-bridge cycle and enhances cardiac performance, presumably via changes in phosphorylation of myosin binding protein C (MyBP-C) and TnI (*1*, *8*, *9*). Alteration in the dynamics of the cross-bridge cycle is one of the molecular mechanisms underlying heart failure. Distinct structural, imaging, biochemical, physical, and molecular studies on the cross-bridge cycle have provided insights into the biological nature of cardiac muscle contractility (*10*−*17*). However, direct quantitative measurements of the attachment/detachment process within the intact sarcomere at the cross-bridge level have not been made (*10*, *15*−*19*).

Several studies show that SPR can be used to investigate biomolecular interactions (*20*−*24*). In the present work, we have therefore modified our previously built SPR system (*25*) to probe cross-bridge interactions in intact sarcomeres (Figure 1). Illumination of a gold film by a laser beam through a prism at incidence angles greater than the critical angle sets up an evanescent electromagnetic wave that interacts with electronic oscillations in the gold film. The surface mode associated with these electronic oscillations is known as the surface plasmon. Resonance excitation occurs when the phase velocity of the evanescent wave matches that of the surface plasmon. At resonance, a major portion of the laser light energy is transferred to the surface plasmon. Thus, the SPR manifests itself as a minimum of the laser reflection (Figure 1) at a specific angle. This SPR minimum angle depends on the wavelength of the laser light and the permittivity of the

† Supported by NIH Grant HL60758 to M.M., Texas Advanced Technology Program to H.S., and Interdisciplinary Research Initiative Award by Texas A&M University (IRI98-50) to M.M. and H.S.

* Corresponding author: office phone 979-847-9251; lab phone 979-862-6503; fax 979-862-4638; e-mail marim@neo.tamu.edu.

‡ Cardiovascular Research Institute and Department of Medical Physiology, College of Medicine, Texas A&M University System Health Science Center.

§ Department of Physics, Texas A&M University.

10.1021/bi0101648 CCC: $20.00
Published on Web 10/25/2001

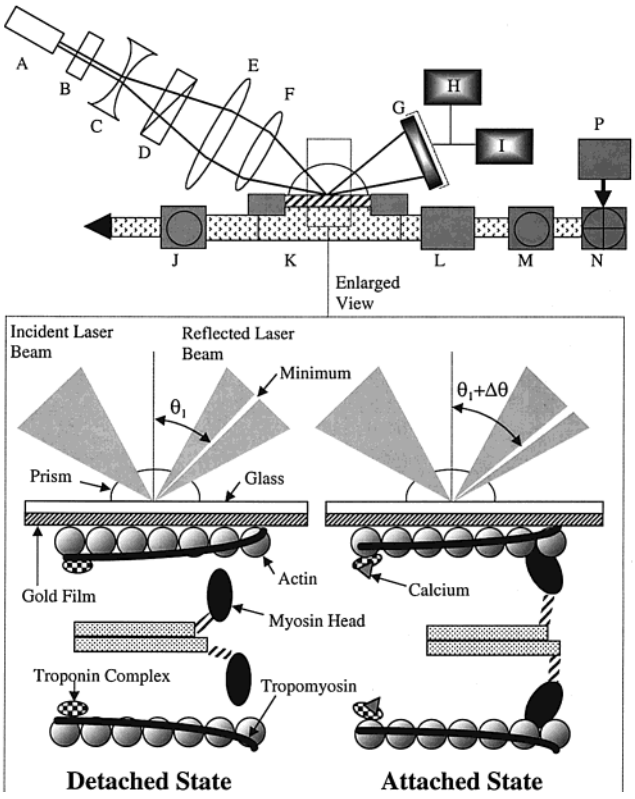

FIGURE 1: Schematic representation of the SPR setup and the SPR detection principle: The optical beam formation unit includes (A) laser, (B) neutral density filter, (C) diverging lens, (D) polarizer, (E) converging lens 1, and (F) converging lens 2. This unit produces a convergent beam. The electronic components include (G) photodiode array, (H) A/D board and computer, and (I) oscilloscope. They serve to register and monitor the reflected light distribution. The fluidic system includes (J) outflow valve, (K) flow cell, (L) temperature controller, (M) inflow and bubble removal valve, (N) multiport selection valve, and (P) syringe-pump. SPR occurs at a specific angle and manifests itself as a minimum in the reflected light distribution. The inherent dielectric permittivity of sarcomeres at a detached state causes the SPR to occur at angle θ_1. When the cross-bridge attachment occurs, it changes the SPR angle by $\Delta\theta$. This is the SPR shift that we observe.

sample medium immediately adjacent to the gold film (*21*, *26*).

The thin and thick filaments of the sarcomeres can be considered a lattice network of dielectric rods with an inherent permittivity. This inherent permittivity determines the initial SPR minimum angle. Cross-bridge attachment between the myosin and the actin is a combination of complementary, hydrophobic, and ionic interactions and hydrogen bonding (*18*). This interaction can change the dielectric permittivity of the sarcomeres. Thus, our hypothesis is that cross-bridge attachment changes the dielectric permittivity of the sarcomere, which then causes a change in the SPR minimum angle. Consequently, SPR measurements on sarcomeres that are immobilized on a gold film can provide an index of the attachment status of cross-bridges within intact sarcomeres (see Figure 1) in response to changing conditions. Unlike other SPR measurements (*22*, *24*), the SPR angle changes that are induced by cross-bridge attachment occur without binding of additional mass to the immobilized protein. A change in the SPR minimum angle will also be referred to as a SPR shift throughout this paper.

Under the condition of our experiments, surface plasmons probe a region corresponding to 2−3 layers of sarcomeres underneath the laser spot. Our results demonstrate that calcium-triggered cross-bridge attachment within the sarcomere induces a positive SPR shift. Furthermore, blocking the cross-bridge cycle at different points to further increase the population of attached cross-bridges yields additional increases in the SPR shift at a constant calcium concentration. Thus our data demonstrate for the first time that SPR measurements monitor cross-bridge attachment/detachment within intact sarcomeres.

MATERIALS AND METHODS

Surface Plasmon Resonance Apparatus. We have adapted our previous surface plasmon resonance configuration (*25*) for measuring the cross-bridge interaction within intact sarcomeres. Figure 1 shows the theoretical basis along with the experimental implementation. A helium−neon laser provides the incident illumination at 633 nm. An arrangement of lenses and a polarizer produces a parallel-polarized light beam that converges at an angular interval, which is adjusted for the observation of SPR with selected dynamic range and resolution. A prism provides coupling of the laser beam to the surface plasmons that are excited in the gold film. A three-channel flow cell allows solution access to the gold film. A photodiode array captures the angular distribution of the reflected light. A data acquisition (DAQ) board AT-MIO-16X (National Instruments) reads the electrical output of the photodiode array and transfers it to a Pentium II-based computer. In-house C++ software calculates in real time the SPR angle and stores the data. Currently, the readout rate of the DAQ board sets the time resolution to 67 ms. The measured beam spot size is 0.15 mm^2. The angular resolution for the configuration used is about 1×10^{-4} deg; this corresponds to 1 resonant unit (RU).

Gold film chips (CM5) coated with carboxymethylated dextran were obtained from BIAcore (Biacore AB, Sweden). When activated, the dextran layer provided a substrate to immobilize sarcomeres via amide bonds. Three-channel flow cells were made to interface with the gold film surface. Each channel has a length of 5 mm, width of 1 mm, and depth of 1 mm. The SPR effect of our system has an estimated penetration depth of 110 nm from the dextran layer to probe the immobilized sarcomeres. A set of valves enabled port selection, bubble removal, and flow cell isolation. A PhD2000 syringe pump (Harvard Apparatus) and manual injection ports provided the fluid flow. A TED200 temperature controller (Profile Optische System GmbH, Germany) regulated the inflow temperature of solutions.

Solutions. The high relaxation (HR) solution contains (in millimoles per liter) $CaCl_2$ 0.025, ethylene glycol bis(*β*-aminoethyl ether)-*N*,*N*,*N*′,*N*′-tetraacetic acid (EGTA) 10, KCl 53.28, $MgCl_2$ 6.81, 3-(*N*-morpholino)propanesulfonic acid (MOPS) 20, ATP 5.35, creatine phosphate (CP) 12. The HR solution serves to keep sarcomeres in a relaxed state through a combination of low [Ca^{2+}] and high [ATP]. The pCa 4.5 solution contains (in millimoles per liter) $CaCl_2$ 9.96, EGTA 10, KCl 33.74, $MgCl_2$ 6.48, MOPS 20, ATP 5.4, and CP 12. A computer program is used to calculate the necessary component concentrations required to achieve the desired free calcium concentration (*27*). With the exception of the

immobilization solutions, all other solutions are adjusted to pH 7.0 with KOH. Protease inhibitors were added to all solutions to the final concentrations of 2.5 mg/L pepstatin, 1.0 mg/L leupeptin, and 50 μmol/L phenylmethanesulfonyl fluoride (PMSF). Calcium concentrations of selected samples of pCa 4.5 solutions were checked by the ratio of fluorescence of Fura-2 pentapotassium salt to 340/380 nm excitation.

Immobilization of Myofibril Preparation onto Gold Film. Mouse cardiac myofibrils were prepared as previously described (*28*), except that all solutions contained protease inhibitors. Total protein concentrations were determined by use of a bicinchoninic acid (BCA) protein estimation kit (Pierce, Rockford, IL).

Injection of a 800 μL solution containing a 1:1 mixture of 0.2 mol/L *N*-ethyl-*N*′-(3-diethylaminopropyl)carbodiimide (EDC) and 0.05 mol/L *N*-hydroxysuccinimide (NHS) from BIAcore's amine coupling kit activated the carboxylated matrix, which covers the gold film and serves as a substrate for immobilization. HR wash followed the 10-min incubation with the activating solution of EDC + NHS. The myofibril suspension was brought to a protein concentration of 0.7 μg/μL, pH between 4.9 and 5.1, at room temperature. The syringe pump then continuously injected the myofibril suspension at the rate of 0.25 mL/min. The temperature controller raised and maintained the temperature of the inflow at 26 °C. Immediately after the immobilization, a HR solution at pH 7.0 was injected. Ethanolamine from the BIAcore amine-coupling kit was not used to consume the remaining activated carboxylated binding sites, since 1.0 mol/L ethanolamine destroyed the ATPase activity of the sarcomeres (data not shown). Alternatively as per the manufacturer's suggestion, 0.1 mol/L Tris at pH 7.0 was used to neutralize the remaining open activated carboxylated binding sites. To verify whether lowering the pH of the myofibril suspension environment for a brief time affected its function, we conducted myofibrillar ATPase assays under similar conditions. The results showed no change in activity (data not shown).

Experimental Protocol. For all of the experiments, the protocol follows the general scheme of (1) obtain baseline measurements on solutions, (2) immobilize sarcomeres, (3) activate sarcomeres, and (4) conduct specific experimental sequences.

We made SPR measurements on the solutions before all subsequent steps to establish solutions-only induced variations. Injections of greater than 5-fold volume of all fluid space provided the total replacement of all previous solution within the SPR apparatus. The SPR measurements were temporarily discontinued during solution injections to eliminate artifacts. After immobilization of the myofibrils, alternating HR and pCa 4.5 solutions were injected to activate the myofibers. This activation cycles were repeated several times until a consistent maximum SPR shift was reached. The phosphate experiment followed the sequential injection of HR, pCa 4.5, and entailed increasing [P_i] by 5−10−15 mmol/L or by 10−20−30 mmol/L at fixed pCa 4.5 solutions. The BDM experiment followed the sequential injection of HR, pCa 4.5, and increases in [BDM] by steps of 2−5−10−20−30 mmol/L at fixed pCa 4.5 solutions. For both increasing [BDM] and [P_i] experiments, SPR measurements in both relaxed and rigor conditions were also made on a subset of experiments. The rigor experiment followed the sequential injection of HR, pCa 4.5, and rigor (pCa 4.5 without ATP and CP) solutions. The high refractive index experiment consisted of activation cycles with both HR and pCa 4.5 solutions containing 0.2 mol/L sucrose. This experiment specifically tested the contribution of the physical contraction by the sarcomeres to the SPR readings. HR injections followed the completion of each experimental sequence. Injection of HR solution containing anti-tropomyosin antibodies at the rate of 0.1 mL/min for 10 min followed the HR wash for some of the experiments to show the presence of sarcomeres on the gold film. Measurements of HR to pCa 4.5 activation-induced SPR shift was made before each group within a sequence. Degradation or loss of this activation SPR response identified damage to sarcomeres; consequently, the experiment was stopped when this occurred. Due to the time constraint of protein viability, no more than two different sequences could be performed on a single channel.

Data Analysis. The mean values and the standard deviations of time segments of the data that corresponded to each experimental event were calculated. The net SPR shift was calculated by subtracting the SPR angle difference of changing solutions only from the SPR angle difference of changing solutions with immobilized protein. Regressions were performed on the processed data. We used ANOVA and Fisher's statistical tests for determining statistical significance between multiple means. The immobilization SPR angle offsets and the noncontributing time segments were removed to allow a side by side comparison of the solutions-only measurements and the measurements of sarcomeres' response to solutions for the appropriate figures. We normalized the SPR shift that was caused by the sarcomere's reaction to the specific experimental condition to the SPR shift that was caused by total amount of immobilization for analysis across different experiments. This ratio will be shown as dP/P throughout this paper.

THEORETICAL BASIS

We use a five-layer model that is based on Maxwell's equations (*29*) describing reflection of light from a layered system to calculate SPR curves, to estimate SPR response from protein immobilization, and to estimate changes in dielectric permittivity due to cross-bridge interaction. The five-layer model consists of the following: first layer, prism with dielectric permittivity $\epsilon_1 = 2.30$; second layer, gold film of thickness $d_2 = 47$ nm with complex permittivity $\epsilon_2 = -13.2 + i1.25$; third layer, dextran layer filled with high relaxation (HR) solution of thickness $d_3 = 140$ nm (*30*) and $\epsilon_3 = 1.78$; fourth layer, sample medium (protein) with thickness d_4 and $\epsilon_4 = 1.96$ (this corresponds to a protein concentration ~40% in an aqueous solution (*30*)); fifth layer, solution only (this layer is assumed to be semi-infinite with respect to the surface plasmon penetration depth). One can obtain the intensity reflection coefficient R for this system with the following recursive equations (*29*) by calculating sequentially each input impedance $Z_{in,m}$ and each layer impedance Z_m:

$$R = \left|\frac{Z_{in,2} - Z_1}{Z_{in,2} + Z_1}\right|^2 \quad (1)$$

The input impedance at layer m ($Z_{in,m}$) and layer impedance

(Z_m) are given by

$$Z_{\text{in},m} = Z_m\left[\frac{Z_{\text{in},m+1} - iZ_m \tan(k_{Z,m}d_m)}{Z_m - iZ_{\text{in},m+1}\tan(k_{Z,m}d_m)}\right] \quad (2)$$

for $m = 2-4$, where

$Z_m = k_{Z,m}/\epsilon_m k_0$ ($m = 1-5$), $Z_{\text{in},5} = Z_5$, $k_{Z,m} = \sqrt{\epsilon_m k_0^2 - k^2}$, $k = k_0\sqrt{\epsilon_1}\sin\theta$, and $k_0 = 2\pi/\lambda$.

The incidence angle θ of the illuminating laser beam onto the prism−gold interface determines the component of the wave vector k that is parallel to the interface. The wavelength of the laser light in a vacuum is λ. A change in dielectric permittivity of the sarcomeres (ϵ_4) will result in a variation of R.

We calculated the decrease of the SPR sensitivity to changes in the dielectric permittivity ϵ_4 with depth z starting from the boundary between the third and fourth layers into the protein sample. This decrease can be approximated as $\sim e^{-z/d_p)}$ with a characteristic penetration depth $d_p = 110$ nm. Assuming the diameter of a sarcomere is ~40 nm (*10*, *31*), one can estimate that SPR measures 2−3 layers of immobilized sarcomeres.

The cross-bridge attachment process in sarcomeres, which includes complementary ionic interactions (*18*), decreases the number of charged particles that can interact with the surface plasmon. Consequently, this change in the net charge can increase the apparent dielectric permittivity (*32*). In accordance with the above equations, the increase in permittivity of the sample layer will cause a positive SPR shift.

RESULTS

Immobilization of Sarcomere on Gold Film. The purified myofibril preparations are immobilized on the gold film that has a carboxylated dextran surface. Figure 2A shows an increase in the SPR angle, which is proportional to the amount of myofibrillar protein being immobilized. The immobilization of the sarcomeres causes SPR shifts ranging from 3 to 24 kRU. This value corroborates well with the estimated value of 25 kRU at saturation according to eqs 1 and 2. An effective immobilization requires the pH to be lower than the isoelectric point of the protein; however, lowering the pH below 4.9 eliminates sarcomeric function and must be avoided. Sarcomeric protein concentrations between 0.5 and 0.75 μg/μL yield an optimal loading. A protein concentration above 1.0 μg/μL promotes a faster immobilization rate; however, it could not be used, since it causes clogging of both the input and the output tubes of the channel at the present flow cell. To further demonstrate that binding of sarcomeres on the gold film caused the observed SPR shift during immobilization, monoclonal anti-TM antibodies (CH1) are injected after both completion of the experiments and subsequent blocking of nonspecific binding with preimmune serum. When the CH1 antibodies bind to all the remaining open TM, the SPR shift exhibits this saturation (Figure 2B). This reaction shows that the sarcomeric proteins are immobilized on the gold film and remain immobilized throughout the preceding experiment.

Calcium Activation of the Sarcomere Causes SPR Shift. To examine whether the SPR system can monitor cross-bridge attachment and detachment, the immobilized sarcomeres are then activated by injecting pCa 4.5 solution. As the thin filament is activated in response to an increase in [Ca^{2+}], the number of attached cross-bridges at dynamic equilibrium should rise. As seen in Figure 3A, flowing replacements of HR solution with pCa 4.5 solution cause positive SPR shifts well beyond the refractive index differences between the solutions themselves. Subsequent replacement of pCa 4.5 solution with HR solution returns the SPR signal back to its baseline value. The increase and the decrease in the SPR minimum angle in the presence of pCa 4.5 and HR solutions, respectively, are repeatable. The magnitude of the pCa 4.5 solution-induced SPR shift directly correlates with the amount of myofibril immobilized on the gold film (Figure 3B). This confirms that SPR shift measurements are a true indication of cross-bridge attachment. Furthermore, using the five-layer theoretical model, we can estimate the apparent change of the dielectric permittivity $\Delta\epsilon$ due to cross-bridge attachment from the experimental data. The observed SPR shift of 120 RU corresponds to $\Delta\epsilon = 1.6 \times 10^{-3}$.

One could argue that the calcium-activated cross-bridge attachment along with lattice space contraction could have produced the SPR shift during the pCa 4.5 activation. To determine whether lattice space contraction contributed any

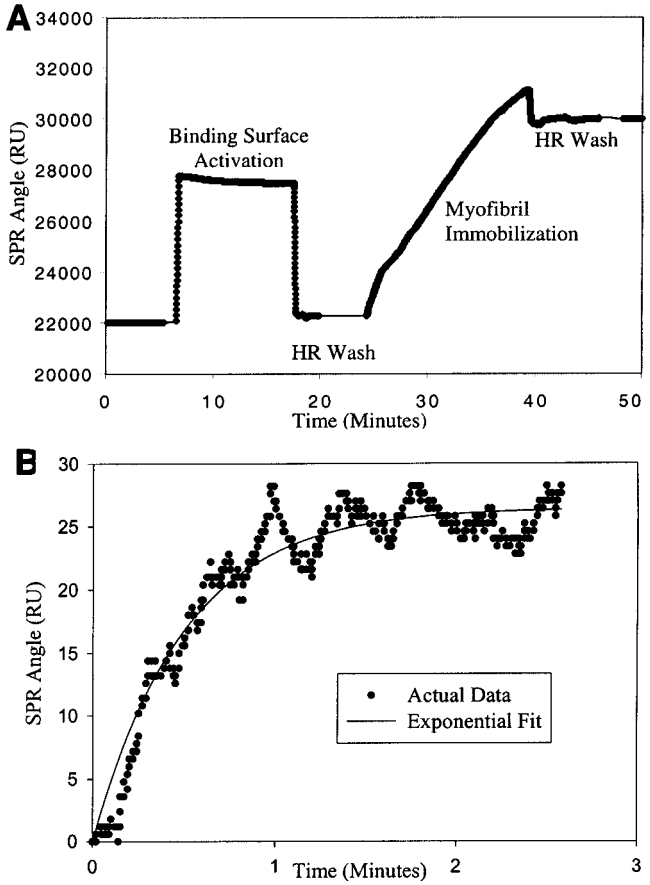

FIGURE 2: Representative sample of the immobilization process: (A) A typical SPR sensorgram documents the immobilization procedure. The increase in the angular position of the SPR shows the binding of sarcomeres onto gold film (HR, high relaxation solution). (B) The positive SPR shift shows anti-TM antibodies binding to immobilized myofibrils during constant flow after preimmune serum block followed completion of an experiment. The binding curve is well fitted by a single-exponential line. The immobilization SPR angle offset and the preceding time segments were excluded for easier visualization.

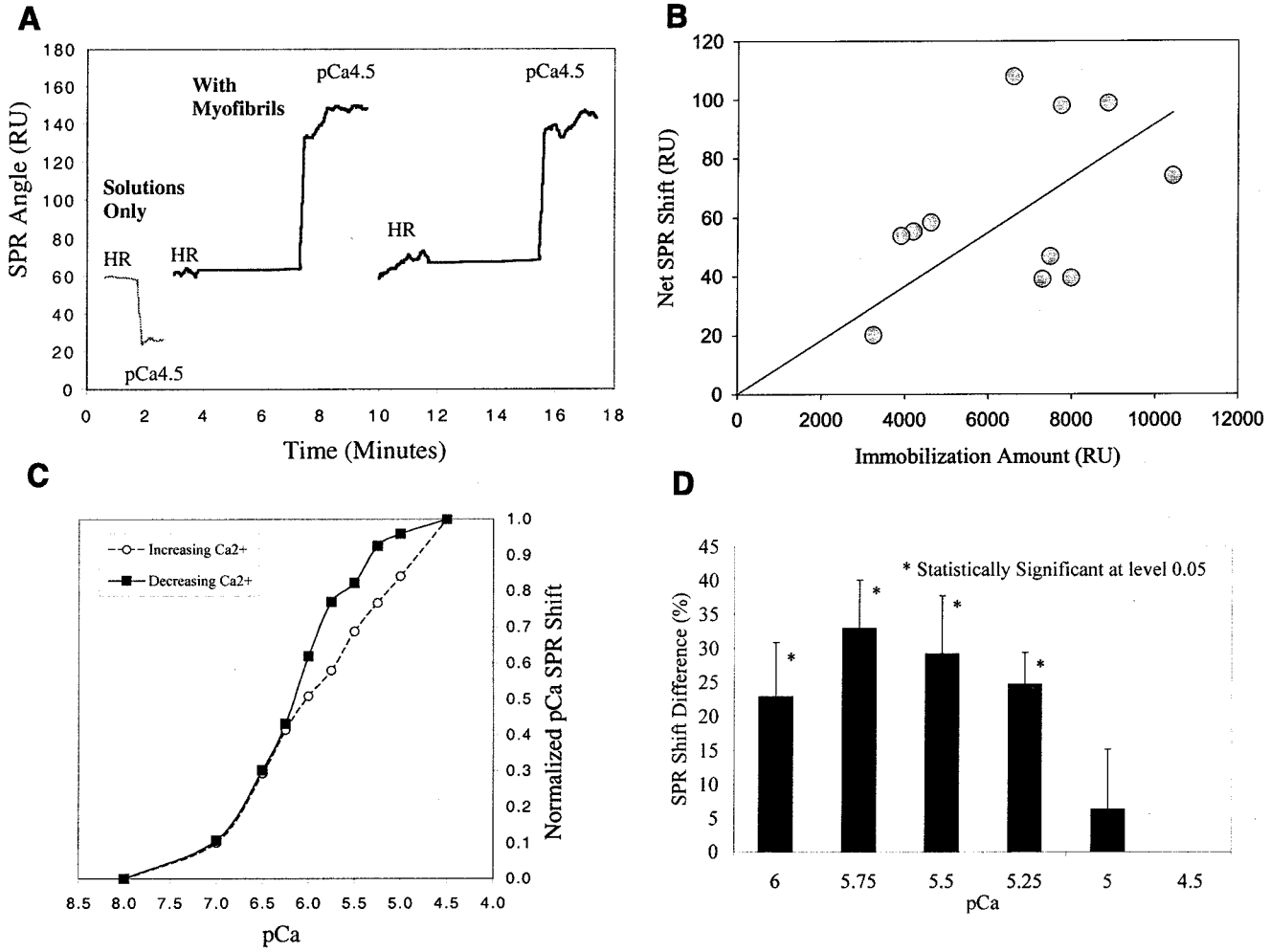

FIGURE 3: Sarcomeres' reaction to changes in $[Ca^{2+}]$ causes SPR shifts: (A) After immobilization of sarcomeres on the gold film, the high relaxation (HR) solution was replaced with pCa 4.5 solution and the SPR response was recorded. The pCa 4.5 solution triggers a SPR shift of greater magnitude with immobilized sarcomeres than for the solutions alone. (B) The relationship between the amount of sarcomere immobilized and the SPR shift is shown (slope of 0.0092). As observed in a series of different experiments, the magnitude of SPR shifts increases with increasing amount of myofibril immobilization. (C) For a fixed myofibril immobilization, this panel shows SPR shifts normalized to maximum shift versus pCa for (○) increasing and (■) decreasing $[Ca^{2+}]$. (D) The percentage difference in the SPR shift at each pCa is calculated as follows: the normalized SPR shift during decreasing $[Ca^{2+}]$ minus the normalized SPR shift during increasing $[Ca^{2+}] \times 100$. Data are presented as mean ± standard error; $n = 3$. The ANOVA test produces $p = 0.031$. Asterisks denote statistical significance at level of 0.05 by Fisher's least significant difference.

SPR shift, we used high refractive index HR and pCa 4.5 solutions that contained 0.2 mol/L sucrose instead of normal solutions for calcium activation. (The difference between pCa 4.5 solutions without and with 200 mM sucrose is approximately 11 000 RU.) It has been shown that addition of up to 600 mM sucrose into Ca^{2+} activating solution does not alter maximum force measurement (*33*, *34*). Scanning electron microscopy on selected samples shows that an average immobilization only covers a fraction of the laser spot of SPR. Thus during pCa 4.5 activation, which causes lattice space contraction, high refractive index solution will enter the SPR measurement region and will amplify the SPR measurement. However, the pCa 4.5 activation-induced SPR shifts in solutions with 0.2 mol/L sucrose was not amplified with respect to shifts in solution without 0.2 mol/L sucrose (data not shown). This indicates that the changes in the lattice spacing within the measurement region during pCa 4.5 activation did not cause noticeable SPR shifts.

To further confirm that the positive SPR shift in the calcium activating solution reflects the population of attached cross-bridges at dynamic equilibrium, we monitor the SPR shift in response to increasing and decreasing $[Ca^{2+}]$. Figure 3C demonstrates that flowing replacements of solutions with increasing $[Ca^{2+}]$ produce a different response curve than flowing replacements of solutions with decreasing $[Ca^{2+}]$. This difference in SPR shifts appears to represent a true hysteresis, as has been demonstrated elsewhere with respect to the force−pCa relationship (*35*). In our measurements, this hysteresis effect is most noticeable between pCa 6.0 and 5.0 (Figure 3D).

Interrupting the Cross-Bridge Cycle at Different Steps of the Cross-Bridge Cycle Can Be Monitored by the SPR System. Since other processes besides calcium binding to thin filament can affect cross-bridge cycling (*36*−*38*), we examined the effects of inorganic phosphate (P_i), 2,3-butanedione monoxime (BDM), and adenosine triphosphate (ATP) on the relative population of attached cross-bridges with SPR. After calcium activation, pCa 4.5 solutions containing various additional concentrations of P_i were injected. The results demonstrate additional positive SPR shifts with increasing $[P_i]$ (Figure 4A). P_i causes a reduction in force by binding to the AM′·ADP state (Figure 7), which then can lead to

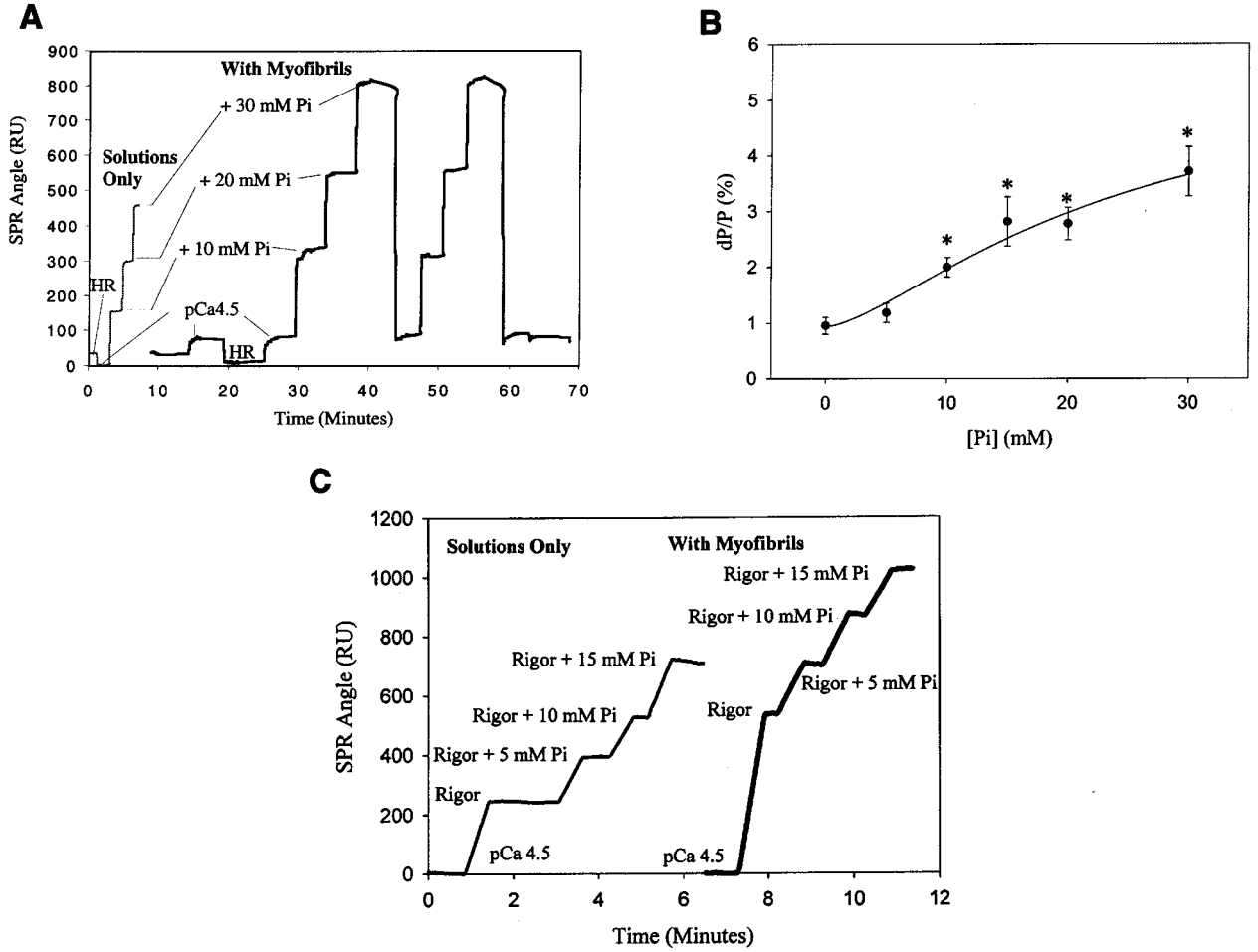

FIGURE 4: Changing the population of the attached cross-bridges by [P_i] causes SPR shifts: (A) The left side of the figure shows SPR measurements on pCa 4.5 solutions only with increasing [P_i]. The right side of the figure shows SPR measurements after immobilization of myofibrils. The differences represent sarcomeres' reactions. (B) This figure summarizes sarcomeres' reactions to increasing [P_i] in pCa 4.5 solution at different amounts of immobilization. The averaged ratio (dP/P) of the magnitudes of sarcomeres' reactions to the amount of sarcomeres that is immobilized versus [P_i] is displayed. The means of the different experiments were fitted to the Hill equation (K_{50} = 23.24 mmol/L). The resultant curve shows that increasing [P_i] causes increasing myofibril reaction with a trend toward saturation. ANOVA−Fisher test was used to compare the multiple means. Asterisks denote significant differences to 0 and 5 mmol/L P_i with $p < 0.001$. Statistical significance does not exist between 15 and 30 mmol/L [P_i] and between 20 and 30 mmol/L [P_i]. Error bars represent standard error of the mean (SEM). (n = 6, 2, 6, 2, 4, and 4 for 0, 5, 10, 15, 20, and 30 mmol/L [P_i] accordingly). (C) Rigor solutions with increasing [P_i] do not cause any appreciable additional SPR shifts.

low force production (*5*, *12*−*14*, *39*−*41*) (see Discussion section for further details). This effect is readily detected as an additional SPR shift even in the presence of a fixed high calcium concentration.

To determine the effect of dose response of [P_i] on SPR shifts, the SPR shifts were normalized to the total amount of sarcomeric protein immobilization (dP/P), as discussed under Materials and Methods. As seen in Figure 4B, the SPR shift trends toward saturation between 20 and 30 mmol/L P_i (fitting to the Hill equation produces K_{50} at 23.24 mmol/L P_i). In addition, the magnitudes of P_i-induced shifts show a positive dependence on the amount of immobilized sarcomeres (data is imbedded in Figure 4B for each [P_i]). Depending on the reference K_a (association constant) and K_{sp} (soluble product) values, a pCa 4.5 solution with more than 25 mmol/L P_i will form a $CaHPO_4$ precipitate. In addition, free [Ca^{2+}] measurements in pCa 4.5 solutions with increasing [P_i] revealed that the free [Ca^{2+}] levels decreased significantly with [P_i] above 30 mmol/L. Due to these reasons, we did not perform any SPR measurements with [P_i] greater than 30 mmol/L; however, Figure 4B shows a decline in the amount of SPR shifts at higher [P_i]. This is well corroborated with previous studies, where slowing of ATP $\leftrightarrow$ P_i exchange rate at 20 mmol/L P_i with continued increases beyond this [P_i] is shown in EDC cross-linked myofibrils (*39*), and tension analysis studies with fibers show continued P_i effects without saturation at 30 mmol/L P_i (*5*, *40*). We have also measured the effect of increasing [P_i] on SPR shifts at both relaxed and rigor conditions. At rigor condition, increasing [P_i] did not show any appreciable SPR shifts (Figure 4C).

Next, we use BDM to investigate whether trapping the cross-bridge cycle at the weak to strong cross-bridge transition step can be detected by SPR measurements as an increase in the population of attached cross-bridges. Figure 5A shows that BDM causes additional SPR shifts in the presence of pCa 4.5 solution. In addition, as seen in Figure 5B, the increasing BDM concentration effect saturates at 20 mmol/L (fitting to the Hill equation produces K_{50} at 11.42 mmol/L; ANOVA−Fisher test shows a lack of significant difference between 20 and 30 mmol/L), which corroborates well with previous studies (*42*, *43*). Furthermore at this BDM

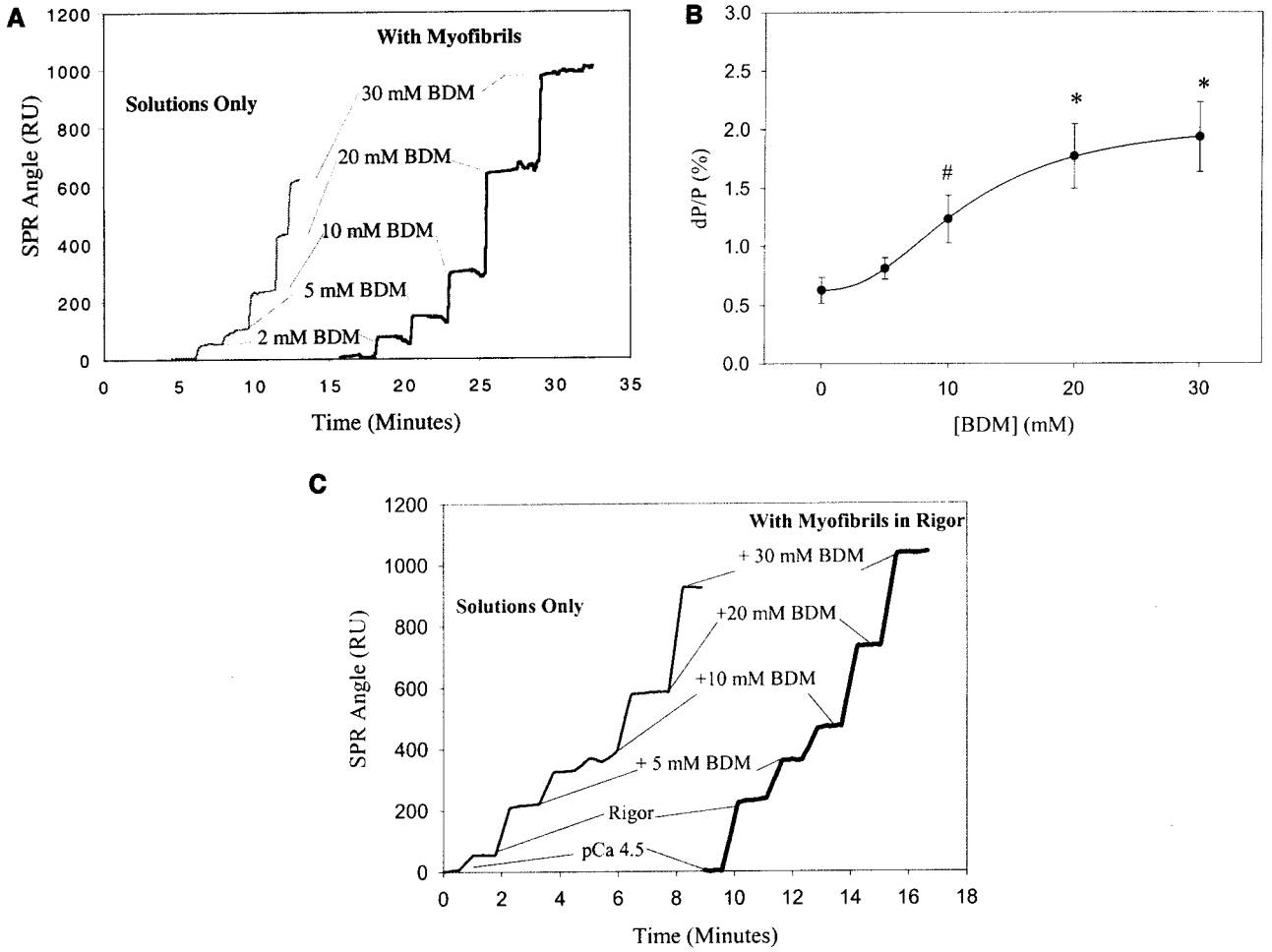

FIGURE 5: Changing the attached cross-bridges by increasing [BDM] causes SPR shifts: (A) This panel provides an example of SPR sensorgrams with increasing [BDM] in the presence of pCa 4.5. The concentration variations trigger greater SPR shifts with immobilized sarcomeres than with solutions alone. (B) This panel summarizes sarcomeres' reactions to increasing [BDM] in pCa 4.5 solution at different amounts of immobilization. The averaged ratio (dP/P) of the magnitudes of sarcomeres' reactions to the amount of sarcomeres that is immobilized versus [BDM] is displayed. The means of the different experiments were fitted to the Hill equation (K_{50} = 11.42 mmol/L). The results show that saturation takes effect with [BDM] at 20 mmol/L. ANOVA−Fisher test was used to compare the multiple means. Asterisks denote significant difference from 0.0 mmol/L BDM by $p < 0.001$ and significant difference from 5 mmol/L BDM by $p < 0.01$. The number sign denotes significant difference from both 0.0 and 30 mmol/L BDM by $p < 0.05$. Error bars represent SEM. n = 6, 6, 5, 5, and 6 for 0, 5, 10, 20, and 30 mmol/L BDM accordingly. (C) Rigor solutions with increasing [BDM] do not cause any appreciable additional SPR shifts.

concentration, there is no appreciable SPR shift under rigor conditions (Figure 5C). Similarly, there are no significant changes with increasing [BDM] and [P_i] in relaxing condition (data not shown). Thus, our data demonstrate that increasing the population of weakly attached cross-bridges with BDM (*43*, *44*) also yields a positive shift in the SPR measurement.

It is well-known that complete ATP depletion in the calcium activating solution can cause all functional cross-bridges to remain in the attached AM state (rigor state, Figure 7). In our experiment, flowing replacements of pCa 4.5 solution with rigor solution causes large SPR shifts (Figure 6A). As illustrated in Figure 6A, subsequent replacement with pCa 4.5 solution returns the SPR reading back to its initial activated state, and then with HR solution the reading returns to the baseline level. As seen in Figure 6B, the rigor-induced SPR shifts are much greater than the SPR shifts caused by pCa 4.5 solution alone or with 30 mmol/L BDM or with 30 mmol/L P_i. In addition, the ratio of normalized SPR shifts at pCa 4.5 to normalized SPR shifts at rigor provides an estimate that 14% of cross-bridges are attached during activation. This suggests the range of 5−30% (values obtained by comparing the lowest and highest SPR shifts of pCa 4.5 and rigor conditions) of cross-bridges are attached to the thin filament during contraction, which correlates with other findings (*15*, *37*).

DISCUSSION

The results presented here provide the first evidence that muscle cross-bridge attachment/detachment within intact sarcomeres can be directly monitored with a SPR system. We demonstrate that the SPR measurements reflect the prevailing population of attached cross-bridges at different steps within the overall cross-bridge biochemical pathways (Figure 7). Despite extensive studies such as X-ray diffraction, electron paramagnetic resonance (EPR), and stiffness measurements to detect cross-bridge attachment status, there is no conclusive evidence that these methods truly reflect the attachment and detachment status of cross-bridges (*15*, *45*−*54*). Therefore, the ability of SPR to directly measure cross-bridge attachment status during contraction and relaxation within intact sarcomere is an important advancement in this field. Monitoring the number of attached cross-bridges

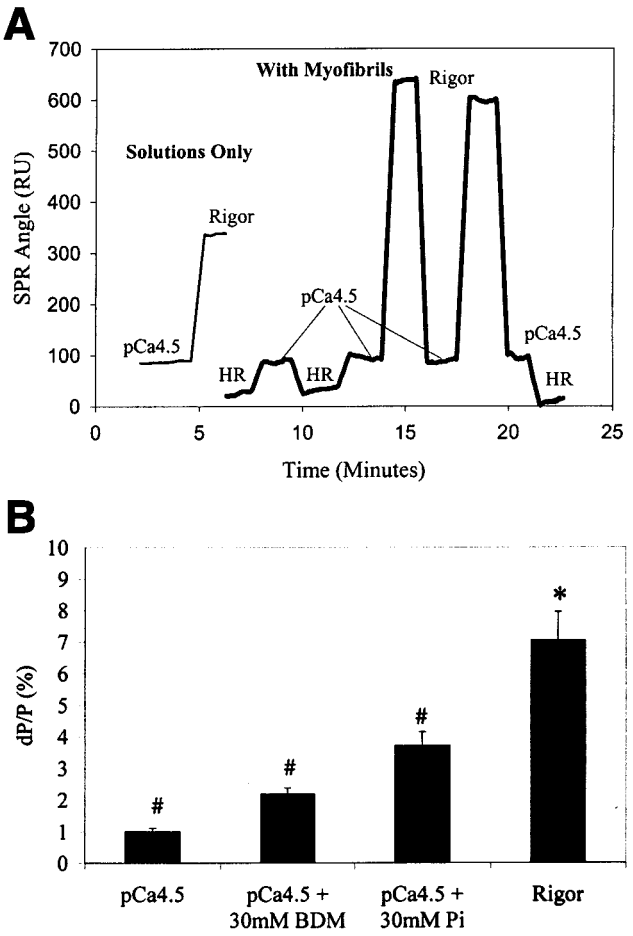

FIGURE 6: Myofibrils' reaction to rigor conditions causes SPR shifts: (A) This panel provides an example SPR sensorgram of the sarcomeres' response transitioning into and out of rigor conditions. Flow sequence of HR−pCa 4.5−rigor solutions causes all available cross-bridges to be attached at the rigor state. Alternating rigor and pCa 4.5 solutions brings cross-bridges into and out of rigor states. Replacement with HR solution return the cross-bridges back to baseline relaxed state. (B) The averaged ratio (dP/P) of the magnitudes of sarcomeres' reactions to the amount of immobilization is shown for pCa 4.5 ($n = 11$), pCa 4.5 with 30 mmol/L [BDM] ($n = 4$), pCa 4.5 with 30 mM [P_i] ($n = 4$), and rigor solutions ($n = 4$). ANOVA−Fisher was used to compare the multiple means. The asterisk denotes that dP/P at rigor is statistically significant from all others with $p < 0.0001$. The number signs denote statistically significant difference from each other with $p < 0.05$.

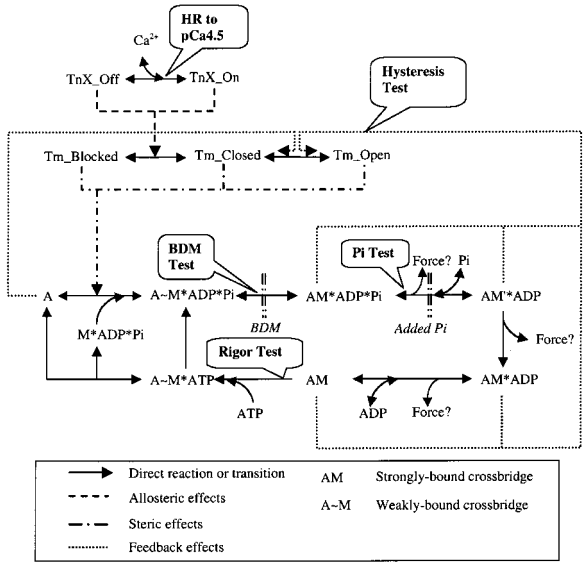

FIGURE 7: Cross-bridge cycle scheme: Calcium binding to TnC causes a conformation change of the entire troponin complex (TnX) from off state to on state (*1*). The TnX at on state moves the TM from blocked to closed state that activates the thin filament (*1*). Myosin (M) hydrolyzes ATP but retains both ADP and P_i (M·ADP·P_i) (*7*). With the thin filament in the calcium-activated state, myosin with hydrolyzed ATP (M·ADP·P_i) can attach to actin (A) forming weakly bound cross-bridges (A∼M·ADP·P_i) (*1*, *2*). Cross-bridge transition from weakly bound state (A∼M...) to strongly bound state (AM...) pushes TM to open state to facilitate further cross-bridge attachment (*2*−*4*, *6*). P_i release is closely associated with force generation (*36*−*38*). AM′·ADP takes what could be considered as irreversible transition to AM·ADP (*12*, *13*). Several opinions exist on the location of force production. One can model force generation taking place at both AM·ADP·P_i and AM′·ADP states (*5*, *38*, *61*). Force production takes place after P_i release (*12*−*14*, *36*, *37*, *39*−*41*). Force production occurs after ADP release (*17*). ATP binding to myosin at the strongly bound state (AM) without residual ADP allows the detachment and the restart of the cycle (*7*). The general overview was originally described by H. E. Huxley (*31*) and A. F. Huxley (*67*). The flags show the five performed tests in the cross-bridge biochemical pathways. The possible positions of where BDM, P_i, and ATP initiate their effects are shown. Additions of BDM and P_i cause redistribution toward prior states.

should yield insights into the molecular mechanism of sarcomere dynamics in cardiac muscle of normal and diseased hearts.

Raising free [Ca^{2+}] around the immobilized sarcomeres on the gold film channel activates the thin filament to increase the number of available actin sites, which then promotes cross-bridge attachment. Taking into account our current understanding of the cross-bridge cycle (see Figure 7), the increase in actin sites should cause an increase in the average number of attached cross-bridges. The increase in SPR shift correlates well with the increase in [Ca^{2+}] of the bathing solution. The dependence of the magnitude of the shift on the extent of the protein immobilization further indicates that the shift is caused by internal protein interactions within sarcomeres. Moreover, the return to the baseline value with a subsequent HR wash follows the expected decrease in cross-bridge attachment due to thin filament deactivation. Finally, the return to baseline and the repeatability of the shift in response to [Ca^{2+}] variations exclude the possibility of the shifts being caused by additional binding of material to the immobilized sarcomeres.

Our hysteresis data provide additional evidence that the increase in the SPR shift during Ca^{2+} activation is due to an increase in the population of attached cross-bridges. Further, the data corroborate the current understanding of the myofilament activation process involving calcium and the formation of strongly bound cross-bridges. The current models show that TM exists in blocked, closed (off), and open (on) states (Figure 7) (*2*, *55*−*58*). In addition to Ca^{2+} binding to TnC, full thin filament activation requires strongly bound cross-bridges (*3*, *4*). Recent three-dimensional reconstruction of electron micrograph data supports the notion that TM requires both calcium and bound myosin to reach the fully activated state (*6*). Thus, calcium activates the Tn complex to allow TM to flex. This flexibility then allows the initial weak binding of myosin to an available actin site. The transition of the cross-bridge from a weakly bound state to a strongly bound state places TM in an open configuration to facilitate further cross-bridge attachment (Figure 7). Thus, sequential action of calcium activation, formation of strongly bound cross-bridge, and feedback occurs for increasing

[Ca^{2+}], which requires higher [Ca^{2+}] to reach 50% maximum force generation. On the other hand, when [Ca^{2+}] is decreased, a lower [Ca^{2+}] can maintain the 50% activity level due to existing strongly bound cross-bridges. This multistep process creates the hysteresis, which is clearly shown in the SPR shifts during Ca^{2+} activation.

The results of increasing [P_i] show SPR measurements can monitor redistribution of cross-bridge populations to attached, but low force-producing, states. Sleep and Hutton (*12*) and Webb et al. (*13*) show that P_i can bind to the high-energy state AM′•ADP (see Figure 7), but not to the lower energy state AM•ADP, to cause redistribution of cross-bridges toward prior states. While this binding of P_i to the AM′•ADP state reduces force production (*5*, *14*, *40*, *59*), cross-bridge attachment remains high (*14*). Several other studies comparing tension to ATPase or tension to stiffness in fiber bundles have also supported this notion (*13*, *39*, *59*, *60*). Thus, considering that the cross-bridge process is a cyclic reaction with the forward rate constants being greater than the reverse rate constants, the net effect of increasing [P_i] probably causes accumulation of cross-bridges in attached, but low force-generating, states. In addition, because of the reversible nature of the cross-bridge cycle, a small amount of redistribution to the other states would also occur with increasing [P_i]. Regnier et al. (*61*) have shown that the largest fraction of redistribution is to the AM•ADP•P_i state. In addition, at activation, increasing [P_i] did not change the EPR spectrum while tension decreased by 70%, suggesting that myosin heads remain attached at the same orientation (*62*). Thus, changes in [P_i] provide an additional method to vary the population of cross-bridges at the attached state. Our data clearly demonstrate that when the thin filament is fully activated, increasing [P_i] causes a further shift in the SPR measurement, which correlates with an increasing number of attached cross-bridges.

Previous studies have shown that BDM either suppresses contraction due to action on the actin−myosin interaction (*42*, *63*−*65*) or inhibits the calcium-regulated attachment to suppress contraction (*60*). It has been shown that BDM acts directly on the myosin molecule (*42*) and increases the rate of ATP hydrolysis but decreases the rate of P_i disassociation from myosin molecule (*43*). Thus, BDM reduces the rate of transition from the non-force-bearing to the force-bearing cross-bridge state with the largest fraction of redistribution to the AM•ADP•P_i state (*61*). Seow et al. (*44*) show that BDM detains cross-bridges in attached but non-force-producing states. Results with BDM show an additional increase in the SPR shift at the maximum [Ca^{2+}], which implies that the SPR measurement can readily detect changes in the population of weakly bound cross-bridges. On the other hand, we observe that rigor solution causes greater SPR shifts that are consistent with increased attached cross-bridge population. In addition, it is interesting to note that there is a very good correlation between the increase in the SPR measurements and the different conditions at which the relative levels of cross-bridges are increased (Figure 6B) (i.e., rigor > P_i effect > BDM effect).

The incongruent effects of P_i or BDM, i.e., reduces the force production and causes accumulation of cross-bridges in the attached but non-force-producing states, allow us to determine whether cross-bridge attachments or lattice spacing changes provide the dominant effect in the SPR measurements. If lattice spacing dominates the SPR measurements, then increasing either P_i or BDM concentrations will decrease the SPR shifts because a reduction in force decreases the amount of lattice space changes in the SPR probed region. On the other hand, if cross-bridge attachment dominates the SPR measurements, then increasing either P_i or BDM will increase the SPR shifts. Our results show that even after subtraction of the SPR shift caused by the solutions alone, an increase in the SPR shift occurred in the presence of P_i or BDM. This clearly demonstrates that cross-bridge attachment dominates the SPR measurements. Cross-bridge attachment via ionic interaction probably alters the net charge within the SPR region to cause permittivity changes. On the contrary, lattice space changes produce little net charge variation within the SPR region. Thus, the SPR detects attachment with greater sensitivity than lattice spacing. However, we cannot rule out the possibility that permittivity changes which have occurred in the presence of either P_i or BDM may be due to conformational changes in the attached cross-bridges upon binding of P_i or BDM, in addition to an increase in the attached cross-bridge population as we have discussed earlier.

Since one can estimate the amount of protein immobilized on the gold film on the basis of the SPR shift [conversion factor 1000 RU/[(ng of protein)mm^2] (*30*)], it is possible to semiquantify the number of cross-bridges from the SPR measurements at rigor conditions. However, one should be cautious about the state of myofibril purification and the amount of functional sarcomeres after the immobilization. The use of SPR also has some limitations. The very shallow penetration depth of 110 nm requires one to place the sarcomeres close to the gold film, which is achieved by the immobilization process. Repeatable rigor-induced SPR shifts identify the total amount of functional cross-bridges and show that possible damage of cross-bridges during immobilization process is not very significant. Others also found that cross-linking myofibrils with EDC did not significantly impact their function (*39*, *66*). In addition, the current method of immobilization does limit the measurement of myofibrils to the isometric condition. However, by increasing the laser wavelength to extend the penetration depth and by improving the fluid system to bring a fiber close enough to the gold film, one can conduct isotonic experiments. The current fluid assembly and data acquisition board (DAQ) with 67 ms time resolution limit the SPR measurements to cross-bridge populations at dynamic equilibrium. However, the planned combination of changing the DAQ to have a 1 ms time resolution and adding UV photolysis will support documenting the kinetics of cross-bridge cycling.

In summary, the results of our experiments with different conditions (Figure 7) to change cross-bridge populations show that SPR provides a method to monitor actin−myosin cross-bridge attachment and detachment within intact sarcomeres. Thus, we have developed a novel experimental technique that can be used to examine the action of inotropic agents that target the myofilaments. In addition, SPR provides a valuable tool to analyze genetically altered mouse models of human diseases, such as familial hypertrophic cardiomyopathy, and for understanding the mechanisms of altered contractility during pathophysiological conditions.

ACKNOWLEDGMENT

Great thanks go to Ms. Niven Boswell for her dedication in many long and arduous experiments. We are grateful to Drs. Michael Davis and Gerald Meininger for their critical evaluation of the manuscript. We also acknowledge Dr. R. John Solaro for his initial advice and encouragement for this study.

REFERENCES

1. Solaro, R. J., and Rarick, H. M. (1998) *Circ. Res. 83*, 471−480.
2. Geeves, M. A., and Lehrer, S. S. (1994) *Biophys. J. 67*, 273−282.
3. Swartz, D. R., Moss, R. L., and Greaser, M. L. (1996) *Biophys. J. 71*, 1891−1904.
4. Fitzsimons, D. P., and Moss, R. L. (1998) *Circ. Res. 83*, 602−607.
5. Millar, N. C., and Homsher, E. (1990) *J. Biol. Chem. 265*, 20234−20240.
6. Vibert, P., Craig, R., and Lehman, W. (1997) *J. Mol. Biol. 266*, 8−14.
7. Lymn, R. W., and Taylor, E. W. (1971) *Biochemistry 10*, 4617−4624.
8. Hoh, J. F., Rossmanith, G. H., Kwan, L. J., and Hamilton, A. M. (1988) *Circ. Res. 62*, 452−561.
9. Winegrad, S. (1999) *Circ. Res. 84*, 1117−1126.
10. Huxley, H. E. (1969) *Science 164*, 1356−1365.
11. Padron, R., and Huxley, H. E. (1984) *J Muscle Res. Cell Motil. 5*, 613−655.
12. Sleep, J. A., and Hutton, R. L. (1980) *Biochemistry 19*, 1276−1283.
13. Webb, M. R., Hibberd, M. G., Goldman, Y. E., and Trentham, D. R. (1986) *J. Biol. Chem. 261*, 15557−15564.
14. Hibberd, M. G., Dantzig, J. A., Trentham, D. R., and Goldman, Y. E. (1985) *Science 228*, 1317−1319.
15. Fajer, P. G., Fajer, E. A., and Thomas, D. D. (1990) *Proc. Natl. Acad. Sci. U.S.A. 87*, 5538−5542.
16. Finer, J. T., Simmons, R. M., and Spudich, J. A. (1994) *Nature 368*, 113−119.
17. Ishijima, A., Kojima, H., Funatsu, T., Tokunaga, M., Higuchi, H., Tanaka, H., and Yanagida, T. (1998) *Cell 92*, 161−171.
18. Rayment, I., Holden, H. M., Whittaker, M., Yohn, C. B., Lorenz, M., Holmes, K. C., and Milligan, R. A. (1993) *Science 261*, 58−65.
19. Lenart, T. D., Allen, T. S. C., Barsotti, R. J., Ellis-Davis, G. C. R., Kaplan, J. H., Franzini-Armstrong, C., and Goldman, Y. E. (1993) in *Mechanism of Myofilament Sliding in Muscle Contraction* (Sugi, H., and Pollack, G. H., Eds.) Plenum Press, New York.
20. Salamon, Z., Wang, Y., Brown, M. F., Macleod, H. A., and Tollin, G. (1994) *Biochemistry 33*, 13706−13711.
21. Salamon, Z., Macleod, H. A., and Tollin, G. (1997) *Biochim. Biophys. Acta 1331*, 117−129.
22. Salamon, Z., Macleod, H. A., and Tollin, G. (1997) *Biochim. Biophys. Acta 1331*, 131−152.
23. Sota, H., Hasegawa, Y., and Iwakura, M. (1998) *Anal. Chem. 70*, 2019−2024.
24. Salamon, Z., Brown, M. F., and Tollin, G. (1999) *Trends Biochem. Sci. 24*, 213−219.
25. Kolomenskii, A. A., Gershon, P. D., and Schuessler, H. A. (1997) *Appl. Opt. 36*, 6539−6547.
26. Raether, H. (1988) *Surface Plasmons on Smooth and Rough Surfaces and on Gratings*, Springer-Verlag, Berlin.
27. Fabiato, A. (1988) *Methods Enzymol. 157*, 378−417.
28. Pagani, E. D., and Solaro, R. J. (1981) in *Methods in Pharmacology*, pp 49−61, Plenum Press, New York.
29. Brekhovskikh, L. M. (1980) *Waves in Layered Media*, 2nd ed., Academic Press, New York.
30. Stenberg, E., Persson, B., Roos, H., and Urbaniczky, C. (1991) *J. Colloid Interface Sci. 143*, 513−526.
31. Huxley, H. E. (1958) *Sci. Am. 199*, 67−82.
32. Shen, L. C., and Kong, J. A. (1983) *Applied Electromagnetism*, Wadsworth, Belmont.
33. Kentish, J. C. (1984) *J. Physiol. 352*, 353−374.
34. Nosek, T. M., and Andrews, M. A. (1998) *Pflugers Arch. 435*, 394−401.
35. Ridgway, E. B., Gordon, A. M., and Martyn, D. A. (1983) *Science 219*, 1075−1077.
36. Goldman, Y. E. (1987) *Annu. Rev. Physiol. 49*, 637−654.
37. Cooke, R. (1997) *Physiol. Rev. 77*, 671−697.
38. Gordon, A. M., Homsher, E., and Regnier, M. (2000) *Physiol. Rev. 80*, 853−924.
39. Bowater, R., and Sleep, J. (1988) *Biochemistry 27*, 5314−5323.
40. Pate, E., and Cooke, R. (1989) *Pflugers Arch. 414*, 73−81.
41. Pate, E., Franks-Skiba, K., and Cooke, R. (1998) *Biophys. J. 74*, 369−380.
42. Higuchi, H., and Takemori, S. (1989) *J. Biochem.* (*Tokyo*) *105*, 638−643.
43. Herrmann, C., Wray, J., Travers, F., and Barman, T. (1992) *Biochemistry 31*, 12227−12232.
44. Seow, C. Y., Shroff, S. G., and Ford, L. E. (1997) *J. Physiol.* (*London*) *501*, 149−164.
45. Malinchik, S., and Yu, L. C. (1995) *Biophys. J. 68*, 2023−2031.
46. Kawai, M., and Brandt, P. W. (1980) *J. Muscle Res. Cell Motil. 1*, 279−303.
47. Ford, L. E., Huxley, A. F., and Simmons, R. M. (1981) *J. Physiol.* (*London*) *311*, 219−249.
48. Pate, E., and Cooke, R. (1988) *Biophys. J. 53*, 561−573.
49. Fajer, P. G., Fajer, E. A., Brunsvold, N. J., and Thomas, D. D. (1988) *Biophys. J. 53*, 513−524.
50. Kraft, T., Yu, L. C., Kuhn, H. J., and Brenner, B. (1992) *Proc. Natl. Acad. Sci. U.S.A. 89*, 11362−11366.
51. Bagni, M. A., Cecchi, G., Colomo, F., and Garzella, P. (1992) *Biophys. J. 63*, 1412−1415.
52. Bartoo, M. L., Linke, W. A., and Pollack, G. H. (1997) *Am. J. Physiol. 273*, C266−276.
53. Veigel, C., Bartoo, M. L., White, D. C., Sparrow, J. C., and Molloy, J. E. (1998) *Biophys. J. 75*, 1424−1438.
54. Stehle, R., and Brenner, B. (2000) *Biophys. J. 78*, 1458−1473.
55. Geeves, M. A., and Halsall, D. J. (1987) *Biophys. J. 52*, 215−220.
56. Maytum, R., Lehrer, S. S., and Geeves, M. A. (1999) *Biochemistry 38*, 1102−1110.
57. McKillop, D. F., and Geeves, M. A. (1991) *Biochem. J. 279*, 711−718.
58. McKillop, D. F., and Geeves, M. A. (1993) *Biophys. J. 65*, 693−701.
59. Regnier, M., and Homsher, E. (1998) *Biophys. J. 74*, 3059−3071.
60. Kagawa, K., Horiuti, K., and Yamada, K. (1995) *Biophys. J. 69*, 2590−2600.
61. Regnier, M., Morris, C., and Homsher, E. (1995) *Am. J. Physiol. 269*, C1532−C1539.
62. Zhao, L., Pate, E., Baker, A. J., and Cooke, R. (1995) *Biophys. J. 69*, 994−999.
63. Yagi, N., Takemori, S., Watanabe, M., Horiuti, K., and Amemiya, Y. (1992) *J. Muscle Res. Cell Motil. 13*, 153−160.
64. Horiuti, K., Higuchi, H., Umazume, Y., Konishi, M., Okazaki, O., and Kurihara, S. (1988) *J. Muscle Res. Cell Motil. 9*, 156−164.
65. Hui, C. S., and Maylie, J. (1991) *J. Physiol.* (*London*) *442*, 527−549.
66. Glyn, H., and Sleep, J. (1985) *J. Physiol. 365*, 259−76.
67. Huxley, A. F. (1957) *Prog. Biophys. Biophys. Chem. 7*, 255−318.

BI0101648